



Year: 2021

Single-cell profiling of myasthenia gravis identifies a pathogenic T cell signature

Ingelfinger, Florian ; Krishnarajah, Sinduya ; Kramer, Michael ; Utz, Sebastian G ; Galli, Edoardo ; Lutz, Mirjam ; Zwicky, Pascale ; Akarca, Ayse U ; Jurado, Nicole Puertas ; Ulutekin, Can ; Bamert, David ; Widmer, Corinne C ; Piccoli, Luca ; Sallusto, Federica ; Núñez, Nicolás Gonzalo ; Marafioti, Teresa ; Schneiter, Didier ; Opitz, Isabelle ; Lanzavecchia, Antonio ; Jung, Hans H ; De Feo, Donatella ; Mundt, Sarah ; Schreiner, Bettina ; Becher, Burkhard

Abstract: Myasthenia gravis (MG) is an autoimmune disease characterized by impaired neuromuscular signaling due to autoantibodies targeting the acetylcholine receptor. Although its auto-antigens and effector mechanisms are well defined, the cellular and molecular drivers underpinning MG remain elusive. Here, we employed high-dimensional single-cell mass and spectral cytometry of blood and thymus samples from MG patients in combination with supervised and unsupervised machine-learning tools to gain insight into the immune dysregulation underlying MG. By creating a comprehensive immune map, we identified two dysregulated subsets of inflammatory circulating memory T helper (Th) cells. These signature ThCD103 and ThGM cells populated the diseased thymus, were reduced in the blood of MG patients, and were inversely correlated with disease severity. Both signature Th subsets rebounded in the blood of MG patients after surgical thymus removal, indicative of their role as cellular markers of disease activity. Together, this in-depth analysis of the immune landscape of MG provides valuable insight into disease pathogenesis, suggests novel biomarkers and identifies new potential therapeutic targets for treatment.

DOI: <https://doi.org/10.1007/s00401-021-02299-y>

Posted at the Zurich Open Repository and Archive, University of Zurich

ZORA URL: <https://doi.org/10.5167/uzh-202960>

Journal Article

Published Version



The following work is licensed under a Creative Commons: Attribution 4.0 International (CC BY 4.0) License.


Originally published at:

Ingelfinger, Florian; Krishnarajah, Sinduya; Kramer, Michael; Utz, Sebastian G; Galli, Edoardo; Lutz, Mirjam; Zwicky, Pascale; Akarca, Ayse U; Jurado, Nicole Puertas; Ulutekin, Can; Bamert, David; Widmer, Corinne C; Piccoli, Luca; Sallusto, Federica; Núñez, Nicolás Gonzalo; Marafioti, Teresa; Schneiter, Didier; Opitz, Isabelle; Lanzavecchia, Antonio; Jung, Hans H; De Feo, Donatella; Mundt, Sarah; Schreiner, Bettina; Becher, Burkhard (2021). Single-cell profiling of myasthenia gravis identifies a pathogenic T cell signature. *Acta Neuropathologica*, 141(6):901-915.

DOI: <https://doi.org/10.1007/s00401-021-02299-y>



Single-cell profiling of myasthenia gravis identifies a pathogenic T cell signature

Florian Ingelfinger^{1,2} · Sinduya Krishnarajah¹ · Michael Kramer³ · Sebastian G. Utz¹ · Edoardo Galli¹ · Mirjam Lutz¹ · Pascale Zwicky¹ · Ayse U. Akarca⁴ · Nicole Puertas Jurado¹ · Can Ulutekin¹ · David Bamert¹ · Corinne C. Widmer⁵ · Luca Piccoli³ · Federica Sallusto^{3,6} · Nicolás G. Núñez¹ · Teresa Marafioti⁴ · Didier Schneider⁷ · Isabelle Opitz⁷ · Antonio Lanzavecchia³ · Hans H. Jung² · Donatella De Feo¹ · Sarah Mundt¹ · Bettina Schreiner^{1,2} · Burkhard Becher¹ 

Received: 13 January 2021 / Revised: 8 March 2021 / Accepted: 17 March 2021
© The Author(s) 2021

Abstract

Myasthenia gravis (MG) is an autoimmune disease characterized by impaired neuromuscular signaling due to autoantibodies targeting the acetylcholine receptor. Although its auto-antigens and effector mechanisms are well defined, the cellular and molecular drivers underpinning MG remain elusive. Here, we employed high-dimensional single-cell mass and spectral cytometry of blood and thymus samples from MG patients in combination with supervised and unsupervised machine-learning tools to gain insight into the immune dysregulation underlying MG. By creating a comprehensive immune map, we identified two dysregulated subsets of inflammatory circulating memory T helper (Th) cells. These signature Th_{CD103} and Th_{GM} cells populated the diseased thymus, were reduced in the blood of MG patients, and were inversely correlated with disease severity. Both signature Th subsets rebounded in the blood of MG patients after surgical thymus removal, indicative of their role as cellular markers of disease activity. Together, this in-depth analysis of the immune landscape of MG provides valuable insight into disease pathogenesis, suggests novel biomarkers and identifies new potential therapeutic targets for treatment.

Keywords Tissue-resident T cells · Biomarker · Autoimmunity · Mass cytometry · Immunophenotyping · Thymus · Myasthenia gravis · Cytokines

Introduction

Myasthenia gravis (MG) is an antibody-mediated autoimmune disease affecting neuromuscular transmission. Most MG patients have autoantibodies recognizing the acetylcholine receptor (AChR), leading to potentially life-threatening muscle weakness [1]. Despite their central role in MG

Bettina Schreiner and Burkhard Becher jointly supervised this work.

✉ Bettina Schreiner
bettina.schreiner@uzh.ch

✉ Burkhard Becher
becher@immunology.uzh.ch

¹ Institute of Experimental Immunology, University of Zurich, Zurich, Switzerland

² Department of Neurology, University Hospital Zurich, Zurich, Switzerland

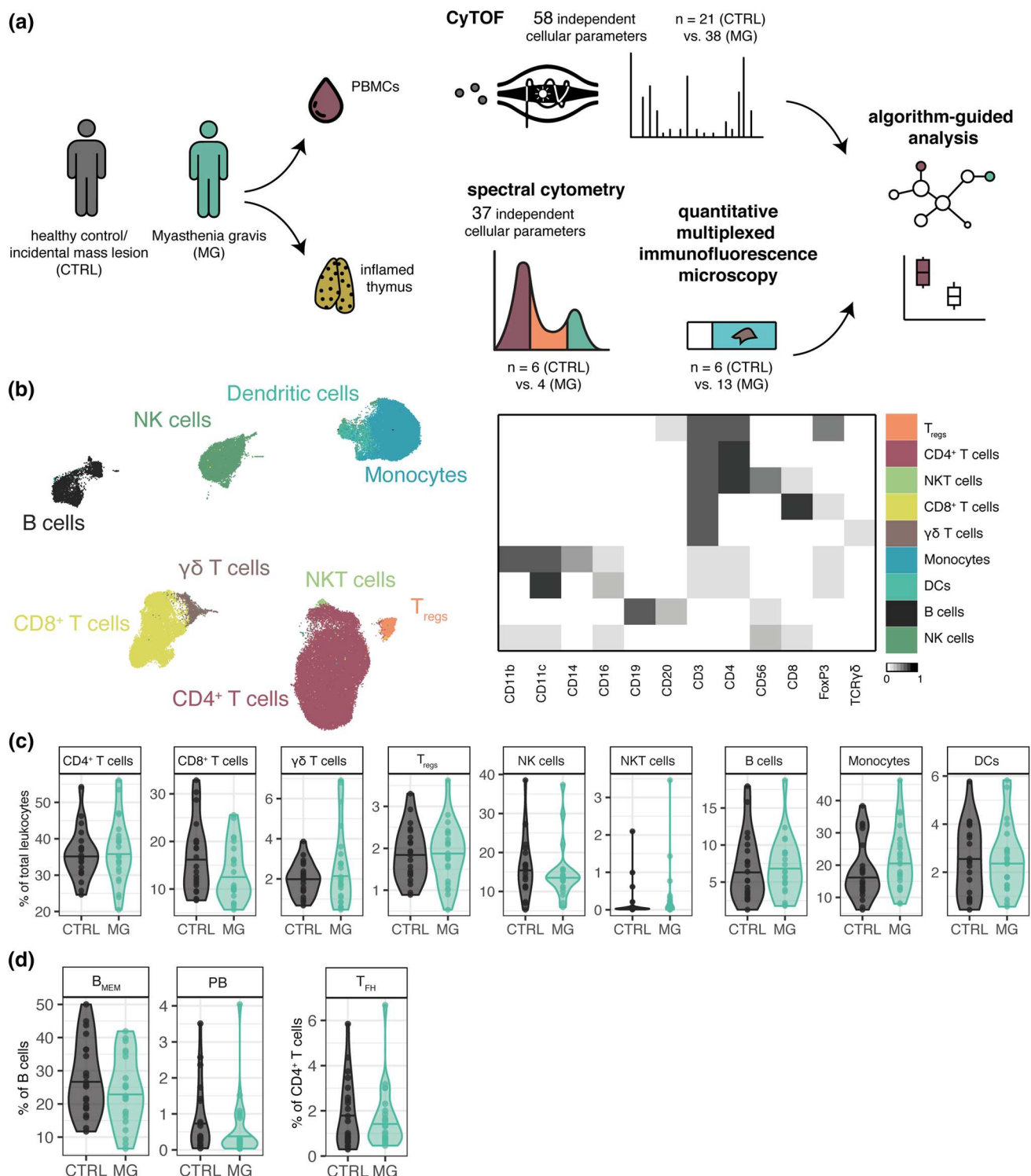
³ Institute for Research in Biomedicine, Università Della Svizzera Italiana, Bellinzona, Switzerland

⁴ Department of Cellular Pathology, University College London Hospital, London, UK

⁵ Department of Medical Oncology and Hematology, University Hospital Zurich and University of Zurich, Zurich, Switzerland

⁶ Institute of Microbiology, ETH Zurich, Zurich, Switzerland

⁷ Department of Thoracic Surgery, University Hospital Zurich, Zurich, Switzerland



pathology, AChR antibody levels do not correlate well with disease severity or treatment responses [37], highlighting our lack of knowledge of the underlying mechanisms of the disease. There is clear evidence of the key role of the thymus in inducing and maintaining MG [23], and several studies have implicated specific cell populations besides

antibody-producing B cells, such as type 1 T helper (Th1) and Th17 cells [21], regulatory T cells (T_{regs}) [2] and follicular Th cells (T_{FH}) [47]. However, a comprehensive unbiased analysis of the immune cells involved in both the thymus and periphery of MG patients is lacking. Here, we employed an immunophenotyping approach to provide insight into the

Fig. 1 The canonical peripheral immune landscape of MG patients does not differ from that of healthy individuals. **a** Cryopreserved peripheral blood mononuclear cells (PBMCs) from myasthenia gravis patients (MG, $n=38$) and healthy controls (CTRL, $n=21$) were labeled with a panel of antibodies recognizing either surface markers or intracellular cytokines (following brief antigen-independent restimulation) and data acquired by CyTOF. Thymic leukocytes from MG patients ($n=4$) and non-MG incidental mass lesion controls ($n=6$) were analyzed in a similar manner by partially overlapping spectral flow cytometry panels. Thymic tissue sections of MG patients ($n=13$) and non-MG controls ($n=6$) were analyzed by quantitative multiplexed immunofluorescence microscopy. The resulting datasets were analyzed using a data-driven high-dimensional approach using supervised and unsupervised machine-learning algorithms. **b** UMAP of 100,000 cells randomly sampled from the combined dataset. Color code indicates FlowSOM clustering and manual annotation according to lineage marker expression profiles presented in the heatmap. T_{reg} s regulatory T cells, DC s dendritic cells, NK natural killer. **c** Violin plots showing the frequency of the FlowSOM-generated immune clusters in healthy controls and MG patients that did not receive immunomodulatory treatment. **d** Violin plots showing the frequency of memory B cells (B_{MEM}), plasmablasts (PB) and peripheral follicular T helper cells (T_{FH}) in healthy controls and MG patients obtained by subclustering the B cell and $CD4^+$ T cell compartments. Violin plots contain a bold horizontal line depicting the respective group mean. If not indicated, the differences between experimental groups were statistically not significant ($p>0.05$) using a nonparametric Mann–Whitney–Wilcoxon test with a false-discovery correction according to the Benjamini–Hochberg approach

cellular and molecular dysregulation leading to autoimmunity in MG patients. By combining mass and spectral flow cytometry with data-driven machine-learning tools, we identified a pathogenic Th cell signature in MG that, unlike autoantibody levels, correlated closely with disease severity. Signature Th cell subsets accumulated in the MG thymus and were restored in the blood after thymectomy. Our study has identified a novel immune signature that upon validation using multicenter large-scale studies could be used as a biomarker to monitor disease severity and inform clinical management of MG patients. Moreover, these results provide a unifying analysis for further interrogation of the cellular mechanisms of MG, and offer the potential to identify novel therapeutic targets for treatment of this disease.

Results

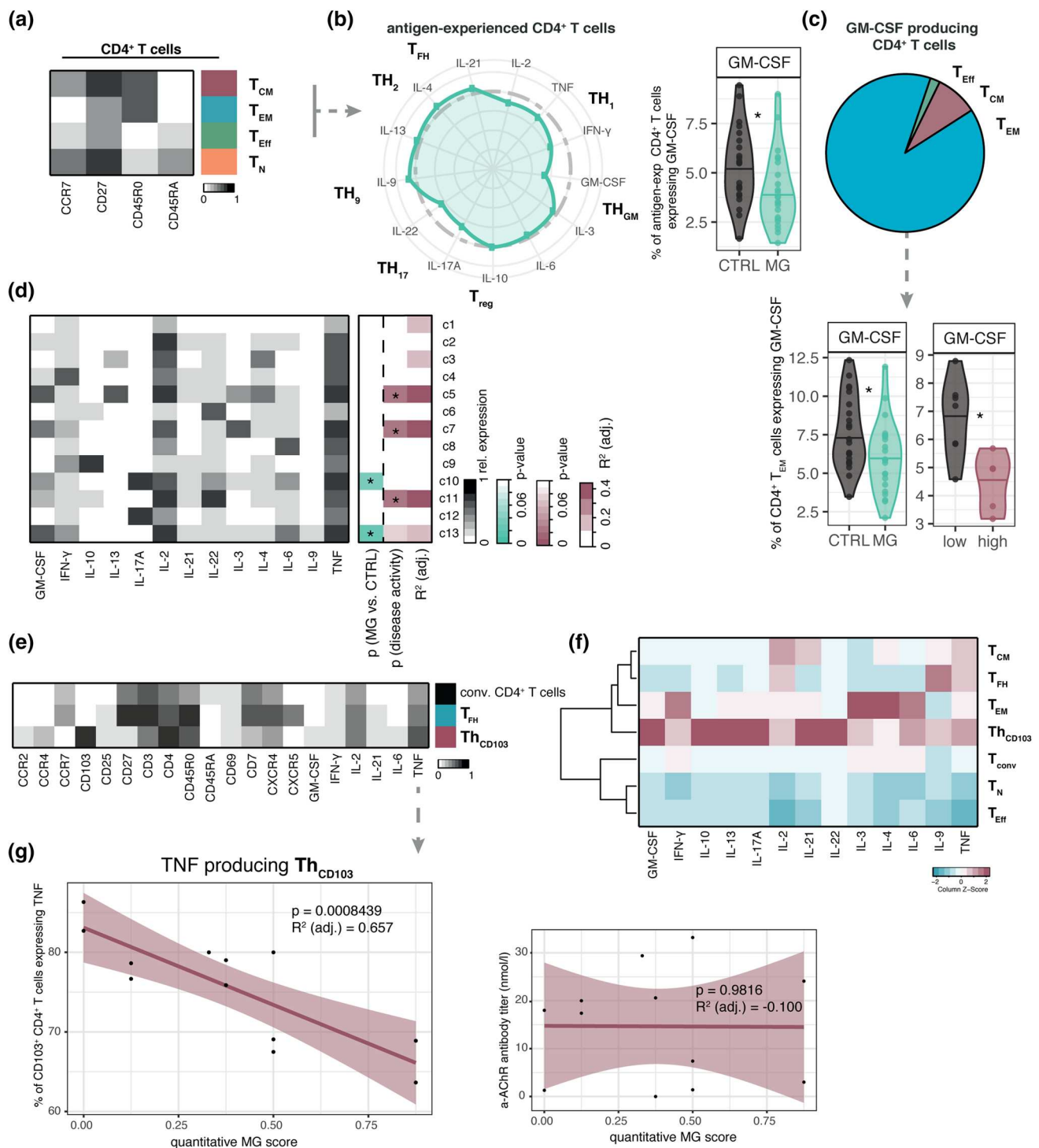
Major blood immune cell populations are comparable in MG patients and healthy controls

To generate a comprehensive immune landscape of the systemic immune compartment in MG, we first analyzed peripheral blood mononuclear cell (PBMC) samples from newly diagnosed steroid-free MG patients and compared them to age- and sex-matched healthy controls (Fig. 1a, Supplementary Data 1). Peripheral blood leukocytes were barcoded and interrogated by partially overlapping mass

cytometry panels to fine-map immune populations with regards to their lineage, trafficking and activation marker expression and the production of 13 different cytokines at single-cell resolution (Fig. 1a, Supplementary Fig. 1a). We then randomly sampled a portion of cells from the combined dataset (100,000 cells) and projected them onto a Uniform Manifold Approximation and Projection (UMAP) [34] for dimensionality reduction (Fig. 1b). FlowSOM, an unsupervised clustering method [19], was employed to describe the most abundant immune populations in the blood: $CD4^+$ T cells, $CD8^+$ T cells, $\gamma\delta$ T cells, T_{reg} cells, natural killer (NK) cells, NKT cells, B cells, monocytes and dendritic cells (Fig. 1b). When we compared the frequencies of these immune cell populations, we found that they were comparable between age- and sex-matched healthy controls and MG patients (Fig. 1c, Supplementary Fig. 1b). Even when we conducted a subset analysis, including those populations previously associated with autoantibody production, such as plasmablasts, memory B cells and T_{FH} cells (Supplementary Fig. 1c), we again did not reveal any frequency differences between patient and control groups (Fig. 1d). Thus, the canonical immune cell composition of blood from MG patients closely resembles that of healthy individuals; this suggests that the pathogenic changes in MG are underpinned either through a functional disturbance of systemic immunity, or through alterations to a locally restricted immune compartment such as the thymus.

Peripheral Th cells of MG patients are characterized by reduced cytokine polarization

We then focused on functional immune profiling by identifying the T cell subsets present in MG and healthy blood, and detecting the cytokines produced by them. We found that $CD4^+$ T cell effector subsets (Fig. 2a, Supplementary Fig. 2a) existed at comparable frequencies in MG patients and healthy controls (Supplementary Fig. 2b). However, when we compared cytokine profiles of antigen-experienced Th subsets [effector Th (T_{Eff}), effector memory Th (T_{EM}) and central memory Th (T_{CM})] we found that MG patients had significantly fewer granulocyte–monocyte colony-stimulating factor (GM-CSF)-expressing cells than healthy controls (Fig. 2b, Supplementary Fig. 2c). The vast majority of GM-CSF-producing Th cells were from the T_{EM} population (Fig. 2c). Strikingly, although the frequency of GM-CSF-producing $CD4^+$ T_{EM} cells was decreased in MG patients in general, it was especially low in the blood of newly diagnosed treatment-naïve MG patients with highly active disease compared to those with mild disease, where MG severity is assessed by the modified quantitative MG score [6] (Fig. 2c, Supplementary Fig. 2d). Thus, it appeared that the GM-CSF-producing $CD4^+$ T_{EM} frequency is significantly dysregulated in MG.



To explore this possibility, we used CD4⁺ T_{EM} cytokine expression data to visualize clusters of cells with specific patterns of cytokine production in the blood of treatment-naïve MG patients and healthy controls. We identified 13 clusters of cytokine-producing cells, of which three were significantly associated with disease severity and two with the disease per se (Fig. 2d, Supplementary Fig. 2e).

Interestingly, all five differentially regulated T_{EM} clusters were those that produced GM-CSF, in combination with tumor necrosis factor (TNF) and interleukin-2 (IL-2). Taken together, despite the inflammatory nature of autoimmune MG, these data clearly show that a general GM-CSF contraction within the T_{EM} population, rather than a specific cytokine profile, characterizes the blood of MG patients.

Fig. 2 Reduced cytokine polarization and systemic TNF-producing CD103⁺ T cells represent an MG-specific signature. **a** Heat map showing relative expression of the indicated activation markers within naïve, memory and effector subsets of CD4⁺ T cells obtained by FlowSOM clustering. **b** Radar plot (left panel) representing the cytokine profile of antigen-experienced CD4⁺ T cell subsets (T_{Eff} , T_{EM} and T_{CM}). The colored line indicates the Cohen's *d* effect size for each cytokine (MG vs. CTRL) as a deviation from the gray dashed reference line. Th cytokine profiles were manually annotated based on partially overlapping key cytokines. The violin plot (right panel) shows the frequency of GM-CSF⁺ cells among antigen-experienced CD4⁺ T cells in control and MG patients. T_{CM} central memory T, T_{EM} effector memory T, T_{Eff} effector T, T_{N} naïve T. **c** Subset composition of the GM-CSF-producing Th cell population within all patients' blood (MG and CTRL; upper panel); and relative abundance of GM-CSF-producing cells within the CD4⁺ T_{EM} population (bottom panel) in control and MG patients (left), and in low and high disease severity newly diagnosed treatment-naïve MG patients (right). Clinical disease severity was determined by the modified quantitative MG score, with low disease severity scoring <0.5, and high disease severity ≥0.5. **d** Cytokine expression analysis of CD4⁺ T_{EM} cells. FlowSOM yielded 13 cytokine expressing clusters (c1–c13; determined by consensus clustering). Corresponding expression profiles (left box) as well as statistical parameters (right box) are displayed. Blue color indicates high significance (low *p* value) for the comparison of treatment-naïve MG patients vs. CTRL, red color indicates high significance and high *R*² value, respectively, for the correlation with the continuous clinical disease severity. **e** Heatmap comparing follicular Th cells (T_{FH}) and CD103⁺ Th cells (T_{CD103}) to conventional Th cells. **f** Row-normalized heatmap of cytokine positivity for 13 detected cytokines among peripheral Th subsets for all patients present in the cohort. **g** Correlation between the frequency of TNF-producing T_{CD103} cells (left panel) or serum anti-AChR antibody titer (right panel) and the modified quantitative MG score as a measure of clinical disease severity for newly diagnosed patients neither receiving immunomodulatory nor symptomatic treatment. Violin plots contain a bold horizontal line depicting the respective group mean. If not indicated, differences between experimental groups were statistically not significant (*p* > 0.05) using a nonparametric Mann–Whitney–Wilcoxon test with a false-discovery correction according to the Benjamini–Hochberg approach. **p* < 0.05. For correlation analysis, statistical parameters were obtained using a linear regression model. Shaded areas in **g** represent the 95% confidence interval

Systemic TNF-producing CD103⁺ Th cells represent a disease-specific signature population, which negatively correlates with the clinical disease severity

Alongside dysregulation of GM-CSF-producing T_{EM} cells, we analyzed trafficking molecules in the Th compartment and found two phenotypically distinct clusters of memory Th cells that were characterized by exclusive expression of the trafficking molecules CXCR5 (T_{FH}) or CD103 (T_{CD103}) (Fig. 2e, Supplementary Fig. 3a and b). We next assessed the functional properties of the identified Th cell subsets in the blood. Interestingly, the blood T_{CD103} population, which has recently been described as a subset of formerly tissue-resident Th cells that have reentered the circulation [29], demonstrated higher frequencies of GM-CSF-, TNF-, IL-17A-, IL-22-, IL-21-, IL-13- and IL-10-producing cells than

any other subset (Fig. 2f, Supplementary Fig. 3c). Moreover, principal component analysis of the cytokine profiles of the Th subsets demonstrated a remarkable heterogeneity in the T_{CD103} compartment, which partially overlapped with T_{FH} cells, T_{EM} cells and T_{CM} cells (Supplementary Fig. 3d). These results indicate that this highly inflammatory subset may have versatile functional properties and a remarkable trafficking capacity, as indicated by the T_{EM} phenotype combined with expression of CCR2, CCR4, CXCR4 and CD103 (Fig. 2e).

Although, overall, MG and control blood contained similar frequencies of T_{CD103} and T_{FH} cells across all Th cell populations (Supplementary Fig. 3e), when we compared MG patients with low and high disease burden, we uncovered a significant inverse correlation between the frequencies of TNF-producing T_{CD103} cells (but for none of the other 12 cytokines analyzed; Supplementary Fig. 4a) and clinical disease severity (Fig. 2g, Supplementary Fig. 4b). In contrast, anti-AChR autoantibody titer in serum, which is the routine blood biomarker for the diagnosis of MG, did not correlate with disease severity (Fig. 2g, right panel). Lastly, we ruled out the possibility that GM-CSF-producing T_{CD103} cells, which demonstrate an overlap with GM-CSF-expressing T_{EM} cells, are solely responsible for the contraction of GM-CSF-expressing Th cells observed in MG (Supplementary Fig. 4c–f).

Collectively, while the overall immune composition in the blood of MG patients did not differ from healthy individuals, we observed consistently lower frequencies of certain patrolling T_{EM} subsets in MG patients, such as GM-CSF-expressing Th cells (T_{GM}) and T_{CD103} cells. This contraction of an inflammatory signature was particularly pronounced in patients with a high disease burden, again counter to our current understanding of the inflammatory processes in MG.

Thymi of MG patients are heavily infiltrated by Th cells and B cells

Given the specific contraction of circulatory T_{CD103} and T_{GM} cells in patients with high disease severity, we speculated whether these cells accumulate in the inflamed thymi of MG patients, characteristic for MG pathology. The thymus of MG patients harbors ectopic germinal centers and high frequencies of autoreactive T and B lymphocytes [4, 5, 41]. To test the notion that the thymus represents the niche wherein those cells reside, we collected thymic tissue from MG patients and sex- and age-matched controls with incidental thymic mass and similar thymus pathology, but without MG (Supplementary Data 2). We compared the CyTOF analysis of the PBMC compartment with the spectral flow cytometry data of the thymic immune landscape by applying the Scaffold framework technique [39]. This computational tool used the immune landscape of the blood as a reference

network onto which the thymic leukocytes were projected (Fig. 3a). FlowSOM clustering was employed in a similar fashion as for the blood analysis to obtain comparable cell populations. Apart from mature leukocytes ($CD4^+$ and $CD8^+$ T cells, B cells, NK cells, NKT cells and myeloid cells), we identified a cluster of developing thymocytes in thymi

(Fig. 3a). Notably, and in line with previous reports supporting a key role for the thymus in maintaining autoreactivity against AChR during MG, we observed that compared to control tissue, MG thymi had relatively higher frequencies of B cells and Th cells, but not cytotoxic $CD8^+$ T cells (Fig. 3b). Furthermore, we observed a significant increase

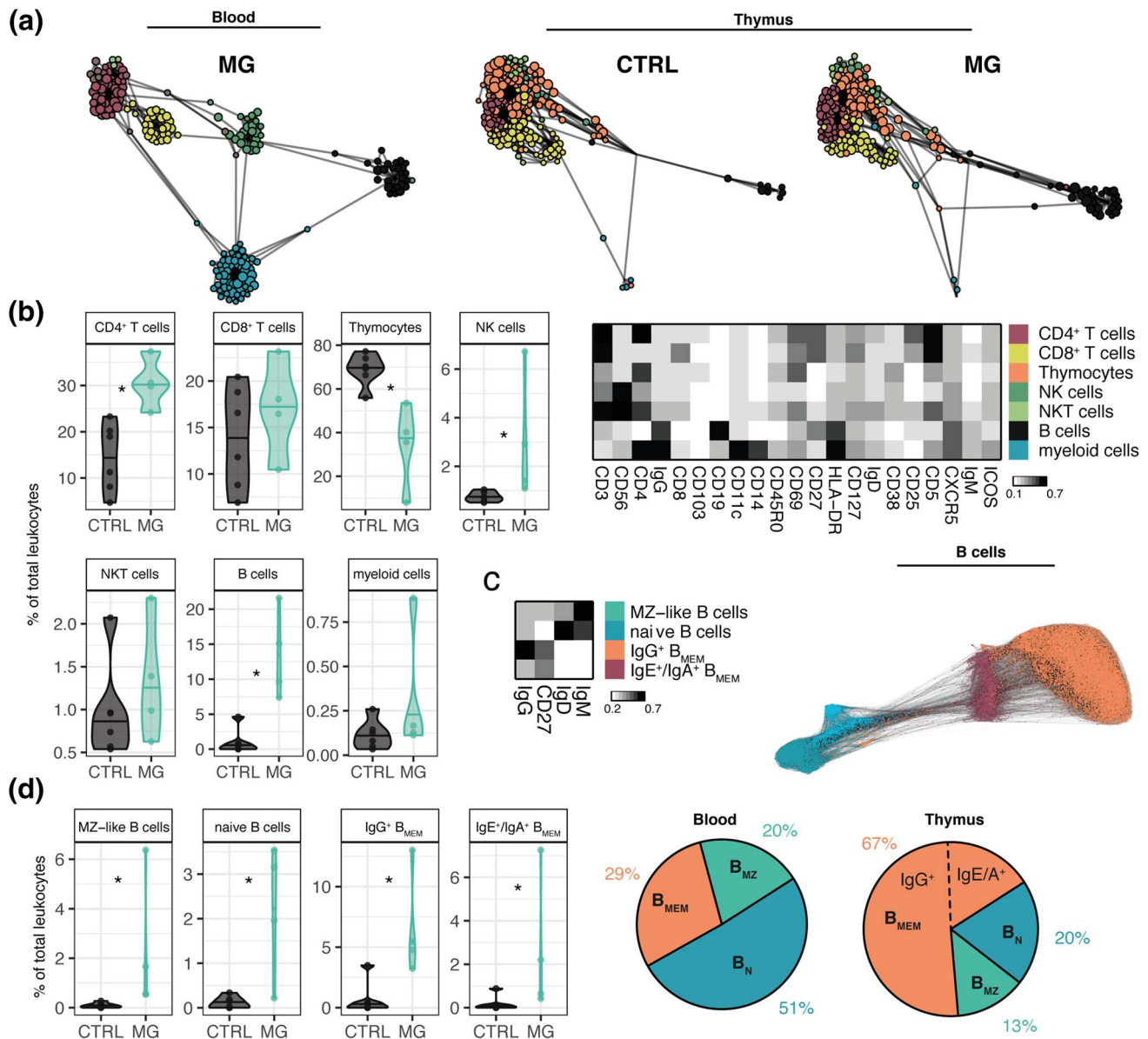


Fig. 3 Thymi of MG patients are infiltrated by Th cells and B cells. **a** Scaffold of the mass cytometry run of the peripheral immune compartment of MG patients and the corresponding maps of the thymic leukocyte landscape of MG patients and non-MG controls determined by flow cytometry. Heatmap below depicts FlowSOM clustering of thymus samples. **b** Violin plots showing frequency of FlowSOM-generated thymic immune clusters for MG patients and incidental non-MG mass lesions. **c** Force-directed layout depicting the network of B cells present in the thymus. Color coding indicates FlowSOM clustering into subpopulations as shown in the heatmap (right panel). *MZ*

marginal zone, B_{MEM} memory B. **d** Violin plots showing frequencies of different B cell subpopulations in the thymus of MG patients and non-MG controls. Pie charts depict the median frequency of peripheral and thymic B cell populations in MG patients. Violin plots contain a bold horizontal line depicting the respective group mean. If not indicated, differences between experimental groups were statistically not significant ($p > 0.05$) using a nonparametric Mann–Whitney–Wilcoxon test with a false-discovery correction according to the Benjamini–Hochberg approach. * $p < 0.05$

in NK cell frequency in MG thymi (Fig. 3b). Control thymi were matched for age (see Supplementary Data 2), thus, the relative decrease of immature thymocytes in thymi of MG patients was likely caused by an influx of circulating leukocytes. First, focusing on B cells (Fig. 3c, d), we observed a significant increase in all subpopulations, including class-switched IgG⁺ and IgE⁺/IgA⁺ memory B cells, in the thymi of MG patients compared to controls (Fig. 3d). Compared to the peripheral blood of MG patients, the MG thymi contained relatively more memory B cells, supporting the concept of a well-defined local inflammatory process underlying autoimmunity in MG (Fig. 3d, right panel).

Medullary regions of the thymi of MG patients are infiltrated by Th_{CD103} and Th_{GM} cells

In accordance with the marked infiltration of class-switched memory B cells, we found increased frequencies of total and IL-21-expressing T_{FH} cells in MG patients compared to controls (Fig. 4a, b, Supplementary Fig. 5a). Enrichment of thymic T_{FH} cells has been described by other studies before and supports the notion of local B cell-supporting T cell pathology [11, 38]. When we measured the overall in situ cytokine profile of antigen-experienced Th cells, we did not find significant alterations in the inflamed thymus of MG patients compared to control thymi (Supplementary Fig. 5b); however, we found a strong trend ($p=0.052$) towards increased frequencies of Th_{GM} cells, the cell population that was specifically contracted in the systemic immune compartment of MG (Fig. 4c). Moreover, we could find Th_{GM} cells in medullary regions of hyperplastic thymi of MG patients (Fig. 4d). Focusing on the other Th cell subset that appeared dysregulated in the blood, we observed that Th_{CD103} signature cells were specifically enriched in the MG thymus. To follow the notion that thymic Th_{CD103} cells represent highly inflammatory tissue-resident memory Th cells that could reenter the circulation and give rise to Th_{CD103} cells found in the peripheral blood, we performed a detailed phenotypic comparison between thymic and blood Th_{CD103} cells, T_{FH} cells and conventional Th cells. In line with previous reports [30, 45, 48], thymic Th_{CD103} cells expressed the tissue-retention molecule CD69 that was absent in the blood counterpart, but demonstrated a shared activated memory phenotype with higher expression of IL-2 and TNF than T_{FH} or conventional Th cells (Fig. 4e, Supplementary Fig. 5c). Furthermore, expression of CCR4 in the Th_{CD103} cluster in the blood (Fig. 4e) supported the migratory capacity of these cells and their ability to sense CCL17 and CCL22; these chemokines are abundant in the thymic medulla where they are secreted by macrophages and dendritic cells and provide medullary entry sites for thymocytes during thymic development [7, 24, 25]. Interestingly, thymic Th_{CD103} cells shared characteristics with T_{FH} cells such as high PD-1 expression

and secretion of IL-21 but could be distinguished from T_{FH} cells due to the absence of ICOS, the higher expression of IL-17A and IL-2 and the exclusive expression of CD103 (Fig. 4e). To increase the number of analyzed samples, we validated the enrichment of Th_{CD103} cells in thymic sections of 13 MG patients and 6 controls by multiplexed quantitative histology and located Th_{CD103} cells within B cell-rich medullary regions of MG thymi (Fig. 4f, Supplementary Fig. 5d–f, Supplementary Data 3). Together with the contraction of TNF-producing CD103⁺ Th cells in the systemic compartment of MG patients, these findings support a pathogenic role of tissue-resident Th cells in locally driven B cell pathology in MG.

Th_{CD103} and Th_{GM} cells rebound in the blood of MG patients after thymectomy

The specific contraction of Th_{CD103} and Th_{GM} cells in the systemic immune compartment in conjunction with an expansion of the signature cells in the inflamed thymus of MG patients points towards a pathogenic local retention of those cells within the inflamed thymus, rather than a global dysregulation of cell frequencies per se. To test this hypothesis, we measured the frequencies of the identified signature subsets in the blood after therapeutic thymectomy; the surgical removal of the inflammatory thymic niche. In thymectomized MG patients, we observed significant decreases in the relative frequency of T_{Eff} coupled with expansion of T_{EM} populations in blood compared to no thymectomy control MG patients (Supplementary Fig. 6a). Notably, the increase of T_{EM} cells after thymectomy followed the opposite trend when comparing MG patients to healthy controls (Supplementary Fig. 2b). Most importantly, we found systemic expansion of the inflammatory signature Th_{CD103} and Th_{GM} populations in athymic patients (Fig. 4g), even though timepoints for blood sampling after thymectomy ranged from several months to several years (Supplementary Data 1). Interestingly, the high levels of the thymus tissue regenerative cytokine IL-22 [14] produced by Th_{CD103} cells were markedly reduced in MG patients previously treated with thymectomy (Fig. 4g, Supplementary Fig. 6b). Since thymectomy released signature cells from the thymus, which could spread to secondary niches such as lymph nodes and bone marrow via blood circulation [16, 17], we lastly investigated whether Th_{CD103} and Th_{GM} cells in the blood were suppressed by standard MG immunotherapy. Due to the lack of targeted immunotherapies in MG, broad immunosuppressive agents like azathioprine, a purine synthesis inhibitor, are administered to stabilize the patients [20]. Coinciding with immunosuppression, we observed a significant reduction in the relative frequency of Th_{CD103} cells in the blood in patients treated with azathioprine (Fig. 4h). Azathioprine even suppressed the rebound of Th_{GM} and Th_{CD103} cells

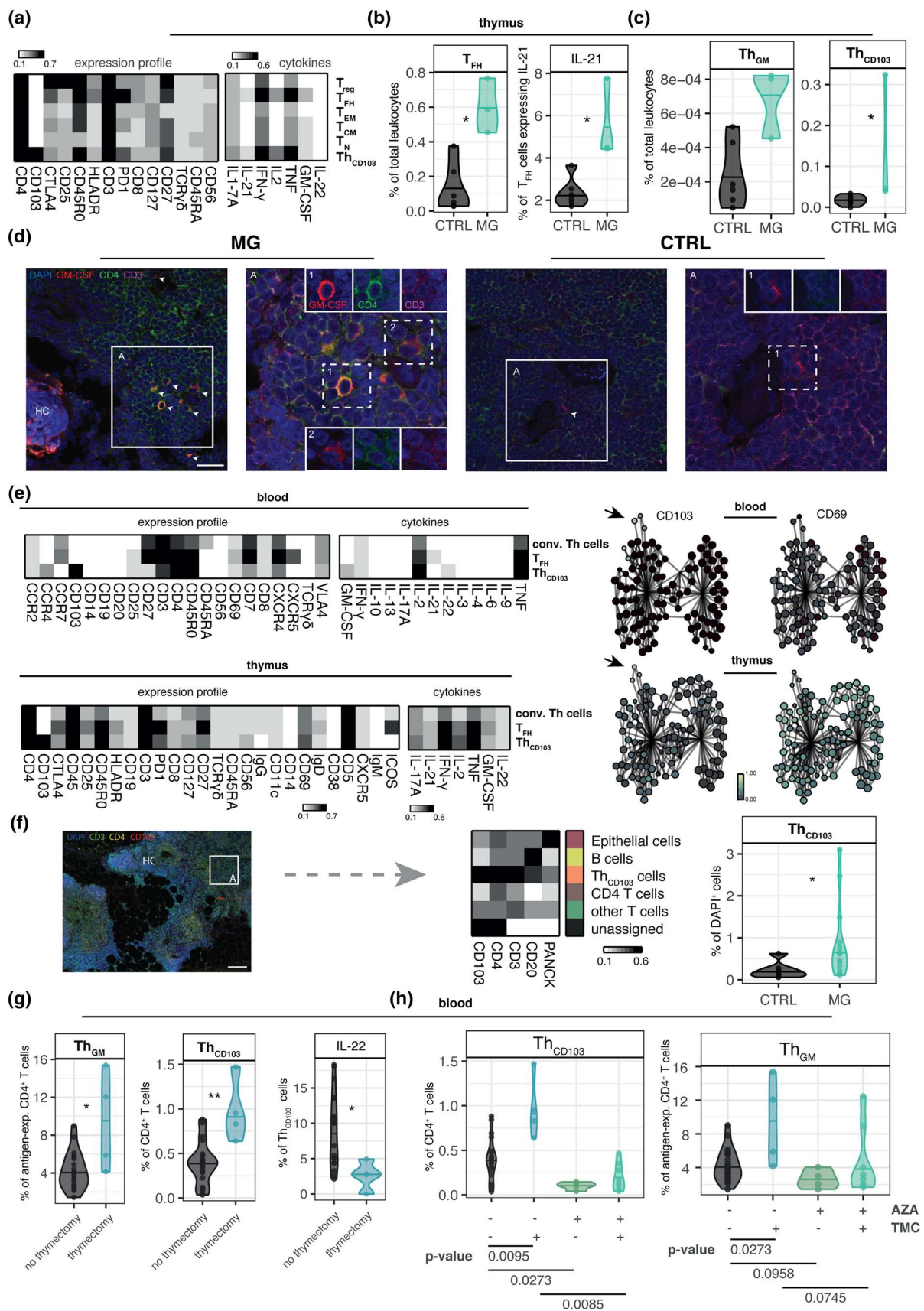


Fig. 4 Signature Th cells are enriched in medullary regions of MG thymus and rebound in the blood after thymectomy. **a** Heatmap of surface markers and cytokine expression profiles of FlowSOM-generated Th subsets. **b** Violin plots comparing the frequencies of T_{FH} cells and the corresponding frequency of IL-21 expression among T_{FH} cells in MG patients vs non-MG patients. **c** Violin plot showing the frequency of GM-CSF expressing Th cells (Th_{GM}) and Th_{CD103} cells in the thymus of MG and non-MG patients. **d** Immunofluorescence labeling of medullary thymic regions showing GM-CSF (red), CD4 (green), CD3 (magenta) and DAPI (blue). Samples from 7 MG patients and 5 non-MG controls were analyzed. Scale bar: 30 μ m. Images of the single labels are enlargements of specified regions. Representative images of two independent experiments (1 slide with 3 sections/patient each) are shown. Left: MG, early onset, female MG patient without immunosuppressive therapy and thymus follicular hyperplasia, right: CTRL, patient with incidental mass, residual thymus tissue. *HC* Hassall's corpuscle. **e** Heatmap of surface markers and cytokine expression profiles of FlowSOM-generated Th subsets in blood and thymus (left panel). Thymic expression profiles from both panels were clustered analogously using FlowSOM and displayed as combined expression profiles. Scaffold of the blood and thymic Th cell compartment in MG patients (right panel). Color overlay depicts expression of CD103 and CD69. **f** Heatmap of expression profiles of FlowSOM-generated cell clusters for quantitative immunofluorescence data of thymic regions after cell segmentation (middle panel). Colors correspond to the populations shown in Fig. S5f. Violin plots showing the frequency of Th_{CD103} cells within DAPI⁺ cells of MG patients and incidental mass lesion controls (right panel). *PANCK* pan-Cytokeratin. **g** Violin plots showing the frequency of Th_{GM} and Th_{CD103} cells, and the frequency of IL-22 production within Th_{CD103} cells, in the blood of MG patients with or without thymectomy that did not receive further immunomodulatory treatment. **h** Violin plots showing the frequency of Th_{CD103} and Th_{GM} cells in the blood of MG patients without treatment or with thymectomy (TMC) and/or azathioprine (AZA) treatment. Violin plots contain a bold horizontal line depicting the respective group mean. If not indicated, differences between experimental groups were statistically not significant ($p > 0.05$) using a nonparametric Mann–Whitney–Wilcoxon test with a false-discovery correction according to the Benjamini–Hochberg approach. * $p < 0.05$; ** $p < 0.01$

driven by thymectomy (Fig. 4h). However, the biggest effect of azathioprine treatment was on the NK cell compartment, especially reducing the $CD56^{dim}$ NK cell population (Supplementary Fig. 6c and d). This observation is in line with the increased risk of azathioprine-treated patients to develop recurrent viral infections and virus-induced malignancies [31] highlighting the need for more tailored therapeutic interventions.

Discussion

Our single-cell profiling study provides novel insights into Th cell-driven MG immunopathology in the thymic niche, and its reflection in the systemic circulation. Using unsupervised machine-learning tools, we identified two subsets of Th cells: Th_{GM} and Th_{CD103} , which were enriched in the inflamed thymus of MG patients, and thus, appeared in lower numbers in the blood. Moreover, the frequencies of

both populations correlated with the clinical disease severity of MG patients, unlike the amount of serum anti-AChR antibodies [37]. In line with the inflammatory phenotype of Th_{GM} cells, a previous study reported GM-CSF as a hallmark cytokine expressed in AChR-reactive Th cells in MG patients [10]. The previous study incorporated antigen-specific T cell libraries and found that, alongside GM-CSF, autoreactive T cells also produced IL-17 and IFN- γ . In addition, we pinpointed IL-22 expression to our signature Th_{CD103} cells, similar to previous findings in skin Th_{CD103} cells [29]. Of note, IL-22 receptor expression is essentially restricted to epithelial and stromal cells, including those of the thymic tissue [13, 14]. Some data suggest that IL-22 has a dual role locally, as it is linked to chronic inflammation but is also essential for thymic regenerative processes limiting tissue injury [14, 46].

Surgical removal of the thymus has long been a standard treatment for MG, and the recently published multicenter randomized MGTx phase 3 trial confirmed the beneficial long-term effects of this procedure compared to oral steroids alone in MG patients [42]. It is thought that its efficacy is based on the removal of ectopic germinal centers and local pathogenic cells that drive the production of anti-AChR autoantibodies [20]. In our study, the signature populations rebounded in the blood after surgical removal of the inflammatory niche supporting the notion of pathological inflammatory leukocyte retention in the thymus during MG. Robat-Jazi and colleagues found significantly decreased IL-22⁺ Th cells in the blood of MG patients after thymectomy (compared to before thymectomy) [35], which is in accordance with our results of reduced IL-22 production by Th_{CD103} cells after removal of the thymus.

From a clinical viewpoint, our study identifies the TNF-producing Th_{CD103} cell subset as a promising candidate as a cellular marker of disease severity in MG which should be validated in further studies. CD103 (integrin $\alpha E\beta 7$) normally retains T cells within epithelial-rich tissues via binding to E-cadherin which is highly expressed in thymic medullary regions [32]. Several investigations have shown that the presence of such cytokine-secreting $CD103^{+}$ tissue-resident memory Th cells is associated with poor outcomes in chronic inflammatory skin diseases such as psoriasis [8], vitiligo [12] and alopecia areata [43]. In addition, in the gut, a potential pro-inflammatory role has been allocated to the Th_{CD103} subset [33]. More recently, Zundler and colleagues reported that $CD103^{+}$ tissue-resident memory Th cells accumulated in the mucosa of patients with inflammatory bowel disease, and that the presence of $CD69^{+} Th_{CD103}$ cells was predictive of flares [48].

Even though the expression of CD103 on T cells has been clearly associated with tissue residency, the function of the circulating $CD103^{+}$ Th population remains considerably less defined. A recent study shed more light on their enigmatic

role, demonstrating that skin-resident CD69⁺ CD103⁺ Th cells can downregulate the tissue-retention marker CD69, reenter the circulation and migrate to secondary human skin locations [29]. This is in accordance with the predominant T_{EM} phenotype, versatile cytokine profile, the broad expression of trafficking receptors and the exclusive expression of CD69 in the tissue but not in the circulation that we observed in the Th_{CD103} cell subset. One might speculate that the circulating properties of both Th subsets represent a shuttle between the origin of disease pathology and secondary sites of chronic pathogenic antibody production (in particular after thymectomy) as suggested by murine xenograft and local infection models [28, 29]. As a proof of principle, we demonstrated that both dysregulated memory Th subsets, Th_{GM} and Th_{CD103}, were indeed effective targets of long-term immunosuppression by azathioprine in steroid-free MG patients. Counter-intuitively, both MG treatment approaches, thymectomy and azathioprine, modulated the frequency of signature cells in the blood in opposite directions, indicating two distinct mechanisms of action. Thymectomy abrogates the retention of inflammatory cells in the thymus thereby increasing signature Th cells in the blood, whereas azathioprine halts cell replication and triggers apoptosis in leukocytes [9]: the combination of these therapies, therefore, both removes pathogenic cells in the thymus and decreases Th signature cells in the circulation. Of note, perioperative high-dose immunosuppression has been shown by others to give a favorable clinical response compared to thymectomy alone [44].

Therefore, novel therapeutic interventions aimed at depleting or reducing Th_{GM} or Th_{CD103} may improve the outcome of MG treatment. One such approach that is currently being developed is the use of specific anti-integrins, controlling both inflammatory effects and immune cell trafficking: Etrolizumab, a monoclonal antibody targeting the two integrins CD103 and $\alpha 4\beta 7$, led to clinical remission in patients with ulcerative colitis in a phase 2 trial, and consecutive phase 3 trials are ongoing [40].

Additional work is required to validate the applicability of the identified signature as a therapeutic target or biomarker for MG disease progression and response to therapy. Due to the heterogeneous nature of the disease, it remains unclear whether the identified Th cell signature is restricted to anti-AChR-antibody-positive MG patients, that we exclusively focused on in this study, or if it can be generalized to other MG forms, not involving the thymus. For example, anti-Muscle-Specific Kinase (MuSK)-positive antibody and seronegative MG patients were not included in this study. In line with this notion, a subject for future studies is to further validate the specificity of the signature compared to other autoimmune diseases such as multiple sclerosis, neuromyelitis optica spectrum disorders or systemic lupus erythematosus. Even though a direct comparison between

the disease signatures is pending, previous studies regarding disease signatures across autoimmune diseases suggest that there is no major overlap [18, 22].

Despite these major limitations, our report represents, to our knowledge, to date the most comprehensive map of the systemic immune compartment and the disease-driving thymus in MG patients. Moreover, it represents a major conceptual advance with the potential to be translated into the clinic, upon further validation using large-scale studies, for the therapeutic targeting of MG, as well as biomarker development.

Materials and methods

Healthy donors and MG patient samples

The study was approved by the Ethics Commission Zurich, Switzerland. MG patients ($n=21$ healthy controls and $n=38$ MG patients) were recruited and upon written informed consent blood and thymus samples were obtained at the Neuromuscular Center and the Department of Thoracic Surgery of the University Hospital Zurich, Switzerland. PBMC and serum samples were isolated at the University of Zurich within 12 h of blood collection. Fresh thymus tissue was obtained from patients undergoing elective thymectomy, in which thymus is routinely discarded ($n=6$ non-MG controls versus $n=5$ MG patients). Furthermore, we retrospectively examined formalin-fixed thymectomy samples provided by the tissue biobank of the Department of Pathology (University Hospital Zurich) by multiplexed immunofluorescence (Supplementary Data 3; $n=6$ non-MG controls and $n=13$ MG patients). Standard histopathological analysis of thymus tissue was performed by a clinical pathologist independent of the study. Samples from both sexes were included in the study. Ages ranged from 23 to 91 years. Diagnosis of MG was based on typical clinical symptoms, a positive anti-AChR antibody test in the serum, a positive electrophysiological measurement, and response to treatment with acetylcholinesterase inhibitors. The diagnosis was confirmed by a neurologist with experience in the care of these patients. No seronegative or anti-MuSK-positive MG patients were included in the study. Healthy controls were age- and sex-matched, had no evidence of acute or chronic infection and were not receiving immunomodulatory therapy. In addition, patients with an (incidental) thymic mass or thymoma and without MG were included in the study (Supplementary Data 2). For the blood comparison of MG patients to healthy controls, only patients that were not treated with immunomodulatory drugs or thymectomy were considered ($n=21$ healthy controls and $n=22$ MG patients). For correlations with the patients' clinical disease, severity exclusively untreated MG patients (excluding symptomatically treated patients; $n=12$)

were considered and the continuous relative quantitative Besinger score was used as a measure of disease severity [6]. The Besinger score is a quantitative MG scoring system that has been adapted and slightly expanded by the MG Foundation of America (MGFA) Task Force for therapy studies (QMG score) [27] and contains similar sub scores (except hand-held dynamometer measurements). When using disease severity as a categorical value, patients demonstrating a relative Besinger score ≥ 0.5 were considered as having high disease severity. For the comparison of thymectomy and/or azathioprine-treated/untreated MG patients, only patients that did not receive further immunomodulatory treatment were considered for the analysis ($n = 20$ non-thymectomized versus $n = 4$ thymectomized; $n = 27$ azathioprine-untreated versus $n = 12$ azathioprine-treated).

Serum anti-AChR autoantibody level measurement

Serum patient anti-AChR autoantibodies were measured at the Department of Clinical Immunology (University Hospital, Zurich) using an ^{125}I radioimmunoassay based on reactivity against fetal and adult nicotinic AChR (DLD Diagnostika), as part of the routine diagnostic procedure.

Leukocyte isolation from blood and thymic tissue

Blood samples were diluted in PBS and PBMC fraction was isolated using SepMate 50 tubes (Stemcell Technologies) and human Lympholyte Separation Medium (Cedarlane). To ensure comparability with PBMC samples, a similar protocol for thymic leukocyte isolation was chosen. In brief, thymic tissue was placed on ice immediately after surgery and processed. A single-cell suspension was achieved by cutting the tissue using a scalpel and syringes. The cell suspension was washed and the leukocyte fraction isolated by density gradient centrifugation using human Lympholyte Separation Medium (Cedarlane). The resulting lymphocyte fraction was washed, cryopreserved in 10% DMSO in fetal calf serum (FCS; Biochrom) and stored in the vapor phase of a liquid nitrogen tank until further analysis.

Ex vivo reactivation of PBMCs

Short-term reactivation of cryopreserved PBMCs or thymic leukocytes and subsequent cytometry analysis were performed as described previously [22]. In short, leukocytes were stored in liquid nitrogen and thawed in a 37 °C water bath before use. Cells were resuspended in cell culture medium [RPMI-1640, 10% FCS (Biochrom), and 1 \times L-glutamine and 1 \times penicillin/streptomycin (both Life Technologies)] supplemented with 1:10,000 benzonase (Sigma–Aldrich), centrifuged (300 \times g, 7 min; 24 °C) and washed twice with cell culture medium. Samples then

underwent antibody labeling, or in the case of intracellular cytokine detection, were rested overnight at 37 °C and restimulated with 50 ng ml $^{-1}$ phorbol 12-myristate 13-acetate (Sigma–Aldrich) and 500 ng ml $^{-1}$ ionomycin (Sigma–Aldrich) in the presence of 1 \times Brefeldin A and 1 \times Monensin (both BD Biosciences) for 4 h at 37 °C before surface marker antibody labeling, fixation, permeabilization and intracellular cytokine antibody labeling.

Antibodies

For mass cytometry, monoclonal anti-human antibodies (Supplementary Table 1) were purchased either conjugated to heavy-metal isotopes (Fluidigm) or were conjugated in house using the MaxPar X8 chelating polymer kit (Fluidigm). Flow cytometry antibodies were purchased already conjugated to the specified fluorochromes (Supplementary Table 2).

Live cell barcoding for mass cytometry

To reduce inter-sample staining variability, minimize sample-handling time, and reduce instrument performance-based signal variation, we made use of a combinatorial live-cell barcoding approach using differentially conjugated anti-CD45 mAbs (Biolegend). MaxPar X8 polymers (Fluidigm) were loaded with six different palladium isotopes (102Pd, 104Pd, 105Pd, 106Pd, 108Pd, and 110Pd) and one indium isotope (115In; all from Trace Sciences International) and conjugated to anti-human CD45 mAbs (BioLegend). To exclude doublets and prevent misidentification of barcodes during debarcoding, a restricted 7-choose-3 approach was applied, resulting in 35 barcodes per mass cytometry run. Independent mass cytometry runs contained equal ratios of MG patients and healthy controls and were subject to randomization with regards to treatment, sex, and age. PBMCs were labeled with heavy metal-tagged CD45 antibodies after ex vivo reactivation at 37 °C for 25 min in cell-staining medium (CSM; RPMI-1640, 4% FCS) on an orbital shaker (500 rpm). Samples were washed twice in CSM and combined into a single reaction vessel for surface marker and cytokine detection.

Surface and intracellular cytokine detection by mass cytometry

The barcoded sample convolute was labeled in 400 μ l CSM containing the antibody mix directed against surface markers for 40 min at 37 °C on an orbital shaker (500 rpm). For dead cell discrimination, 2.5 μ M cisplatin (Sigma–Aldrich) was added for 2 min on ice.

For transcription factor detection, the sample convolute was fixed and permeabilized for 40 min at 4 °C in 1X

FOXP3 Fixation/Permeabilization Buffer (BioLegend). Sample was washed in permeabilization buffer [(PBS, 0.5% saponin, 2% bovine serum albumin (BSA), 0.01% sodium azide (all Sigma-Aldrich)] and nuclear staining was performed in 400 µl permeabilization buffer for 1 h at 4 °C.

For intracellular cytokine detection the sample convolute was fixed in 1.6% paraformaldehyde (Electron Microscopy Sciences) for 1 h at 4 °C. The convolute was washed with permeabilization buffer and labeled with antibodies recognizing intracellular cytokines in 400 µl permeabilization buffer for 1 h at 4 °C.

In both the cases, the labeled and stained sample mix was washed and resuspended in 1X iridium intercalator solution (Fluidigm) followed by a 4 °C incubation overnight. Finally, the sample was washed twice with PBS and twice with Max-Par water (Fluidigm) before data acquisition.

Flow cytometry sample labeling and data acquisition

Flow cytometry labeling was performed similarly as for mass cytometry. In brief, samples were labeled with 100 µl of a fluorochrome-conjugated antibody mix in PBS for 20 min at 4 °C and washed twice in PBS. For intracellular cytokine detection, samples were fixed for 20 min at 4 °C using 100 µl Cytofix/Cytoperm (BD Biosciences). Cytokine staining was performed in 100 µl antibody mix in permeabilization buffer at 4 °C overnight. Samples were washed twice and acquired at a Cytex Aurora Spectral Analyzer (Cytex Bioscience). Quality control on a daily basis ensured reliability and reproducibility of the machine's performance.

Compensation matrix was corrected in FlowJo (TreeStar) and samples were gated into live CD45⁺ singlets and exported to the R analysis framework.

Mass cytometry acquisition and data preprocessing

Barcoded and labeled sample data were acquired on a CyTOF 2.1 mass cytometer (Fluidigm). Instrument quality control and tuning was performed on a daily basis. Acquisitions from two independent runs were normalized using five-element beads (Fluidigm) [15]. To further control for batch effects, each independent run contained one normalization control sample that was present in both runs. Live single cells in the sample convolute were identified based on event length, center, width, DNA (¹⁹¹Ir and ¹⁹³Ir) and live/dead (¹⁹⁵Pt) channels in FlowJo (TreeStar). Debarcoding was achieved by Boolean gating in FlowJo of cells exclusively bearing three barcodes. Both flow and mass cytometry data were transformed in the R environment using an inverse hyperbolic sine (arcsin) function. In case individual markers were not aligned in the normalization controls of both mass cytometry runs due to residual batch effects, cofactors

of the sample convolute were adapted to achieve the same mean in staining intensity for both normalization controls. A channel-based percentile normalization using the 99.9th percentile was further applied on the transformed dataset for flow and mass cytometry data. Cytokine positivity was determined in an automated fashion by calculating the 99th percentile of the residual cytokine labeling of an unstimulated control.

Immunohistochemistry

Thymus tissue samples were cryosectioned for immunohistochemistry using a Hyrax C60 cryostat (Zeiss). Thymus sections (10 µm) were fixed with 2% (wt/vol) paraformaldehyde (PFA) in 0.1 M phosphate buffer, pH 7.4, and acetone, washed in PBS, and blocked with PBS supplemented with 0.1% Triton X-100 and 4% normal goat serum. Subsequently, sections were incubated with the following primary antibodies (diluted in blocking solution) overnight at 4 °C: rat anti-GM-CSF antibody (BD Pharmingen, clone BVD2-21C11, 1:50), mouse anti-CD4 antibody (Biolegend, clone RPA-T4, 1:50) and rabbit anti-CD3 (NOVUS, clone SP7, 1:100). Sections were then washed in PBS and incubated with AF647-labeled goat anti-rat, AF488-labeled goat anti-mouse and AF555-labeled goat anti-rabbit secondary antibodies (Life Technologies, 1:500) overnight at 4 °C. Sections were mounted with SlowFade Gold antifade reagent with DAPI (Invitrogen). Fluorescence photomicrographs were captured with a SP5 Leica confocal laser scanning microscope (SP5; Leica) equipped with argon and helium lasers using the 40× objective lens (oil immersion, NA1.25). Images were processed and merged by Imaris imaging software (Bitplane).

Multiplexed immunofluorescence

Multispectral immunofluorescence was performed applying the following antibody panel to Formalin-fixed paraffin-embedded tissue sections of thymus and normal tonsil tissues: CD3 (Leica Microsystems Ltd, clone LN10, 1:50), CD4 (Leica Microsystems Ltd, clone 4B12, 1:50), CD20 (Leica Microsystems Ltd, clone L26, 1:200), CD23 (Leica Microsystems Ltd, clone 1B12, RTU), CD103 (Abcam, clone EPR4166(2), 1:500), Cytokeratin (Agilent Technologies, clone AE1/AE3, 1:100), and counterstaining with DAPI. The optimized multiplexed immunofluorescence protocols were validated against chromogenic singleplex protocols on consecutive sections of a normal human reactive tonsil tissue and thymus samples. Prior to staining, all tissue slides were deparaffinised on the Leica BOND RX automated immunostainer (Leica Microsystems) by soaking in BOND Dewax solution at 72 °C and then rehydrating in ethanol. Tyramide signal amplification-based Opal method

was used in this study for immunofluorescence (IF) staining (Opal 7-Color Automation IHC Kit, Akoya Biosciences). The primary antibody conditions and order of staining determined using DAB detection were directly applied to the fluorescent assays. Unlike conventional immunohistochemistry, a chromogenic peroxidase substrate is used for antigen detection, each antibody is paired with an individual Opal fluorophore for visualization. Importantly, if biomarkers were expected to co-localize in the same cellular compartment then they were paired with spectrally separated Opals. In addition, low expressing markers were coupled to more intense Opals to facilitate spectral acquisition, and vice versa. The Opal fluorophores were used at a 1/100 to 1/200 dilutions. As such, a fluorescent singleplex was performed for each biomarker and compared to the appropriate chromogenic singleplex to assess staining performance.

All fluorescently labeled slides were scanned on the Vectra 3 at 20× magnification using appropriate exposure times. Initially, whole slide images were scanned with all five standard epi-fluorescence filters (DAPI, FITC, Cy3, Texas Red and Cy5). Then, when MOTiF Opals were solely used, images were acquired using tile scanning with the mIF whole slide unmixing filters (DAPI + Opal 570/690, Opal 480/620/780, and Opal 520). Library slides were generated from representative tissue sections to allow for accurate unmixing of the multiplexed samples, including a slide stained for each single fluorophore, a DAPI only slide, and an autofluorescence slide wherein no antibody, Opal reagent or DAPI was applied. For quantification of tissue sections, cells were segmented based on the DAPI signal using the inForm 2.3 software (PerkinElmer) and imported into the statistical programming environment R. Downstream analysis including transformation, dimensionality reduction and cell clustering was carried out analogous to the cytometry analysis described below.

In addition, for individual representative CD103 stainings of thymi, immunohistochemistry was performed using the two-step IHC staining kit EnVision + System HRP DAKO (Glostrup, Denmark) according to the manufacturer's instructions. Sections underwent heat-mediated antigen retrieval with Dako Target Retrieval Solution. DAB was used as the chromogen, and the sections counterstained with haematoxylin and analyzed with the light microscope Olympus BX41.

Algorithm-guided high-dimensional analysis

The high-dimensional analysis was accomplished in the R environment. For FlowSOM clustering, 100 clusters were generated from the combined dataset and metaclustered based on the elbow point. The elbow point was determined by plotting the percentage of variance explained in relation to the number of metaclusters using the package

ConsensusClusterPlus. UMAPs were generated using the R package *umap* with default settings [34]. Force-directed layouts were generated using the ForceAtlas2 algorithm [26] integrated in the Vortex graphical clustering environment creating unweighted edges between the nodes based on the 10 nearest neighbors [36]. Resulting graphs were further modified using the Gephi Toolkit 0.9.2. Scaffold networks were created using the improved version of the initial *Scaffold* package consisting of *grappolo*, *vite* and *panorama* [39]. Mass cytometry FlowSOM nodes of the peripheral blood were used to create the landmark nodes. All plots and visualizations were drawn using the *ggplot2* package.

Statistical analysis

Immune cell frequencies were compared using the unpaired nonparametric Mann–Whitney–Wilcoxon test using the *stats* package. To correct for multiple testing, the Benjamini–Hochberg correction was applied [3]. Linear regression analysis was carried out using the R base function *lm*.

Supplementary Information The online version contains supplementary material available at <https://doi.org/10.1007/s00401-021-02299-y>.

Acknowledgements We thank all our patients who contributed to this study and made this work possible. We are grateful to our clinical neuromuscular team and assistants, including Dr. Ina Reichen, and day-clinic nurses for their support. We thank Dr. Lucy Robinson from Insight Editing London for manuscript editing. This work was funded by grants from the Olga Mayenfisch Foundation (to B.S.), Swiss Foundation of Muscle Diseases (FSRMM; to B.S. and F.I.) and Betty and David Koetser Foundation for Brain Research (to B.S.), the Swiss National Science CRSII5_183478 (to B.B.) foundation, the European Research council (ERCAdG_IMPACT to B.B.). F.I. received a Ph.D. fellowship from the Studienstiftung des deutschen Volkes.

Author contributions FI designed and performed all the cytometry experiments and performed the bioinformatic analysis of the data. SK helped with mass cytometry experiments and data analysis. EG helped with panel design and acquisition of the mass cytometry experiments. BS, SGU, AUA and TM performed all the histological analysis. SGU, PZ, and NGN helped with panel design for spectral cytometry experiments. MK and LP cloned antibodies. SM and FI assessed in vivo pathogenicity of antibodies. BS, FI, ML, SK, and NPJ isolated and processed patient samples. CU and DB helped with the analysis. BS, HHJ, IO, DS and CCW selected and characterized the patient cohorts. AL and FS supervised antibody cloning and production. DDF provided intellectual, scientific and clinical input. SM provided intellectual and scientific input. BB and BS jointly supervised and funded the study. FI, BS and BB wrote the manuscript.

Funding Open Access funding provided by Universität Zürich.

Data availability Raw mass and spectral flow cytometry data are available at <https://doi.org/10.17632/nkcb8nc7w8.1>.

Code availability Code of the bioinformatic analysis pipeline is available at https://github.com/florianingelfinger/MG_publication.

Declarations

Conflict of interest The authors declare no competing interests.

Open Access This article is licensed under a Creative Commons Attribution 4.0 International License, which permits use, sharing, adaptation, distribution and reproduction in any medium or format, as long as you give appropriate credit to the original author(s) and the source, provide a link to the Creative Commons licence, and indicate if changes were made. The images or other third party material in this article are included in the article's Creative Commons licence, unless indicated otherwise in a credit line to the material. If material is not included in the article's Creative Commons licence and your intended use is not permitted by statutory regulation or exceeds the permitted use, you will need to obtain permission directly from the copyright holder. To view a copy of this licence, visit <http://creativecommons.org/licenses/by/4.0/>.

References

1. Alshekhlee A, Miles JD, Katirji B, Preston DC, Kaminski HJ (2009) Incidence and mortality rates of myasthenia gravis and myasthenic crisis in US hospitals. *Neurology*. <https://doi.org/10.1212/WNL.0b013e3181a41211>
2. Balandina A, Lécart S, Darteville P, Saoudi A, Berrih-Aknin S (2005) Functional defect of regulatory CD4⁺CD25⁺ T cells in the thymus of patients with autoimmune myasthenia gravis. *Blood*. <https://doi.org/10.1182/blood-2003-11-3900>
3. Benjamini Y, Hochberg Y (1995) Controlling the false discovery rate: a practical and powerful approach to multiple testing. *J R Stat Soc Ser B*. <https://doi.org/10.1111/j.2517-6161.1995.tb02031.x>
4. Berrih-Aknin S, Cohen-Kaminsky S, Lepage V, Neumann D, Bach JF, Fuchs S (1991) T-cell antigenic sites involved in myasthenia gravis: correlations with antibody titre and disease severity. *J Autoimmun*. [https://doi.org/10.1016/0896-8411\(91\)90013-3](https://doi.org/10.1016/0896-8411(91)90013-3)
5. Berrih-Aknin S, Morel E, Raimond F, Safar D, Gaud C, Binet JP et al (1987) The role of the thymus in myasthenia gravis: immunohistological and immunological studies in 115 cases. *Ann N Y Acad Sci*. <https://doi.org/10.1111/j.1749-6632.1987.tb51282.x>
6. Besinger UA, Toyka KV, Hömberg M, Heininger K, Hohlfeld R, Fateh-Moghadam A (1983) Myasthenia gravis: long-term correlation of binding and bungarotoxin blocking antibodies against acetylcholine receptors with changes in disease severity. *Neurology*. <https://doi.org/10.1212/wnl.33.10.1316>
7. Bleul CC, Boehm T (2000) Chemokines define distinct microenvironments in the developing thymus. *Eur J Immunol*. [https://doi.org/10.1002/1521-4141\(2000012\)30:12%3c3371::AID-IMMU3371%3e3.0.CO;2-L](https://doi.org/10.1002/1521-4141(2000012)30:12%3c3371::AID-IMMU3371%3e3.0.CO;2-L)
8. Boyman O, Conrad C, Tonel G, Gilliet M, Nestle FO (2007) The pathogenic role of tissue-resident immune cells in psoriasis. *Trends Immunol*. <https://doi.org/10.1016/j.it.2006.12.005>
9. Broen JCA, van Laar JM (2020) Mycophenolate mofetil, azathioprine and tacrolimus: mechanisms in rheumatology. *Nat Rev Rheumatol*. <https://doi.org/10.1038/s41584-020-0374-8>
10. Cao Y, Amezcua RA, Kleinstein SH, Stathopoulos P, Nowak RJ, O'Connor KC (2016) Autoreactive T cells from patients with myasthenia gravis are characterized by elevated IL-17, IFN- γ , and GM-CSF and diminished IL-10 production. *J Immunol*. <https://doi.org/10.4049/jimmunol.1501339>
11. Çebi M, Durmus H, Aysal F, Özkan B, Gül GE, Çakar A et al (2020) CD4⁺ T cells of myasthenia gravis patients are characterized by increased IL-21, IL-4, and IL-17A productions and higher presence of PD-1 and ICOS. *Front Immunol*. <https://doi.org/10.3389/fimmu.2020.00809>
12. Cheuk S, Schlums H, Gallais Sérézal I, Martini E, Chiang SC, Marquardt N et al (2017) CD49a expression defines tissue-resident CD8⁺ T cells poised for cytotoxic function in human skin. *Immunity*. <https://doi.org/10.1016/j.immuni.2017.01.009>
13. Dudakov JA, Hanash AM, Van Den Brink MRM (2015) Interleukin-22: immunobiology and pathology. *Annu Rev Immunol*
14. Dudakov JA, Hanash AM, Jenq RR, Young LF, Ghosh A, Singer NV et al (2012) Interleukin-22 drives endogenous thymic regeneration in mice. *Science* (80-). <https://doi.org/10.1126/science.1218004>
15. Finck R, Simonds EF, Jager A, Krishnaswamy S, Sachs K, Fantl W et al (2013) Normalization of mass cytometry data with bead standards. *Cytom Part A*. <https://doi.org/10.1002/cyto.a.22271>
16. Fujii Y, Monden Y, Hashimoto J, Nakahara K, Kawashima Y (1985) Acetylcholine receptor antibody-producing cells in thymus and lymph nodes in myasthenia gravis. *Clin Immunol Immunopathol*. [https://doi.org/10.1016/0090-1229\(85\)90018-2](https://doi.org/10.1016/0090-1229(85)90018-2)
17. Fujii Y, Monden Y, Hashimoto J, Nakahara K, Kawashima Y (1985) Acetylcholine receptor antibody production by bone marrow cells in a patient with myasthenia gravis. *Neurology*. <https://doi.org/10.1212/wnl.35.4.577>
18. Galli E, Hartmann FJ, Schreiner B, Ingelfinger F, Arvaniti E, Diebold M et al (2019) GM-CSF and CXCR4 define a T helper cell signature in multiple sclerosis. *Nat Med*. <https://doi.org/10.1038/s41591-019-0521-4>
19. Van Gassen S, Callebaut B, Van Helden MJ, Lambrecht BN, Demeester P, Dhaene T et al (2015) FlowSOM: using self-organizing maps for visualization and interpretation of cytometry data. *Cytom Part A*. <https://doi.org/10.1002/cyto.a.22625>
20. Gilhus NE (2016) Myasthenia gravis. *N Engl J Med* 375:2570–2581. <https://doi.org/10.1056/NEJMra1602678>
21. Gradolatto A, Nazzari D, Truffault F, Bismuth J, Fadel E, Foti M et al (2014) Both Treg cells and Tconv cells are defective in the myasthenia gravis thymus: roles of IL-17 and TNF- α . *J Autoimmun*. <https://doi.org/10.1016/j.jaut.2013.12.015>
22. Hartmann FJ, Bernard-Valnet R, Quériault C, Mrdjen D, Weber LM, Galli E et al (2016) High-dimensional single-cell analysis reveals the immune signature of narcolepsy. *J Exp Med*. <https://doi.org/10.1084/jem.20160897>
23. Hohlfeld R, Wekerle H (2008) Reflections on the “intrathymic pathogenesis” of myasthenia gravis. *J Neuroimmunol*
24. Imai T, Baba M, Nishimura M, Kakizaki M, Takagi S, Yoshie O (1997) The T cell-directed CC chemokine TARC is a highly specific biological ligand for CC chemokine receptor 4. *J Biol Chem*. <https://doi.org/10.1074/jbc.272.23.15036>
25. Imai T, Chantry D, Raport CJ, Wood CL, Nishimura M, Godiska R et al (1998) Macrophage-derived chemokine is a functional ligand for the CC chemokine receptor 4. *J Biol Chem*. <https://doi.org/10.1074/jbc.273.3.1764>
26. Jacomy M, Venturini T, Heymann S, Bastian M (2014) ForceAtlas2, a continuous graph layout algorithm for handy network visualization designed for the Gephi software. *PLoS ONE*. <https://doi.org/10.1371/journal.pone.0098679>
27. Jaretzki A, Barohn RJ, Ernstoff RM, Kaminski HJ, Keeseey JC, Penn AS et al (2000) Myasthenia gravis: recommendations for clinical research standards. *Neurology*
28. Jiang X, Clark RA, Liu L, Wagers AJ, Fuhlbrigge RC, Kupper TS (2012) Skin infection generates non-migratory memory CD8⁺ T RM cells providing global skin immunity. *Nature*. <https://doi.org/10.1038/nature10851>

29. Klicznik MM, Morawski PA, Höllbacher B, Varkhane SR, Motley SJ, Kuri-Cervantes L et al (2019) Human CD103⁺ CD4⁺ cutaneous resident memory T cells are found in the circulation of healthy individuals. *Sci Immunol* 4:eaav8995. <https://doi.org/10.1126/sciimmunol.aav8995>
30. Klicznik MM, Morawski PA, Höllbacher B, Varkhane SR, Motley SJ, Kuri-Cervantes L et al (2019) Human CD4⁺CD103⁺ cutaneous resident memory T cells are found in the circulation of healthy individuals. *Sci Immunol*. <https://doi.org/10.1126/sciimmunol.aav8995>
31. Komiya A, Kawai H, Yamada S, Kato M, Yanagisawa M, Miyagawa Y et al (1987) A killing defect of natural killer cells with the absence of natural killer cytotoxic factors in a child with Hodgkin's disease. *Blood*
32. Kutleša S, Wessels JT, Speiser A, Steiert I, Müller CA, Klein G (2002) E-cadherin-mediated interactions of thymic epithelial cells with CD103⁺ thymocytes lead to enhanced thymocyte cell proliferation. *J Cell Sci*
33. Lamb CA, Mansfield JC, Tew GW, Gibbons D, Long AK, Irving P et al (2017) α E β 7 integrin identifies subsets of pro-inflammatory colonic CD4⁺ T lymphocytes in ulcerative colitis. *J Crohns Colitis*. <https://doi.org/10.1093/ecco-jcc/jjw189>
34. McInnes L, Healy J, Saul N, Großberger L (2018) UMAP: uniform manifold approximation and projection. *J Open Source Softw*. <https://doi.org/10.21105/joss.00861>
35. Robat-Jazi B, Hosseini M, Shaygannejad V, Nafissi S, Rezaei A, Mansourain M et al (2018) High frequency of Tc22 and Th22 cells in myasthenia gravis patients and their significant reduction after thymectomy. *NeuroImmunoModulation*. <https://doi.org/10.1159/000490855>
36. Samusik N, Good Z, Spitzer MH, Davis KL, Nolan GP (2016) Automated mapping of phenotype space with single-cell data. *Nat Methods*. <https://doi.org/10.1038/nmeth.3863>
37. Sanders DB, Burns TM, Cutter GR, Massey JM, Juel VC, Hobson-Webb L (2014) Does change in acetylcholine receptor antibody level correlate with clinical change in myasthenia gravis? *Muscle Nerve*. <https://doi.org/10.1002/mus.23944>
38. Song Y, Zhou L, Miao F, Chen G, Zhu Y, Gao X et al (2016) Increased frequency of thymic T follicular helper cells in myasthenia gravis patients with thymoma. *J Thorac Dis*. <https://doi.org/10.21037/jtd.2016.03.03>
39. Spitzer MH, Gherardini PF, Fragiadakis GK, Bhattacharya N, Yuan RT, Hotson AN et al (2015) An interactive reference framework for modeling a dynamic immune system. *Science* (80-). <https://doi.org/10.1126/science.1259425>
40. Vermeire S, O'Byrne S, Keir M, Williams M, Lu TT, Mansfield JC et al (2014) Etrolizumab as induction therapy for ulcerative colitis: a randomised, controlled, phase 2 trial. *Lancet*. [https://doi.org/10.1016/S0140-6736\(14\)60661-9](https://doi.org/10.1016/S0140-6736(14)60661-9)
41. Vincent A, Thomas HC, Scadding GK, Newsom-Davis J (1978) In-vitro synthesis of anti-acetylcholine-receptor antibody by thymic lymphocytes in myasthenia gravis. *Lancet*. [https://doi.org/10.1016/S0140-6736\(78\)90073-9](https://doi.org/10.1016/S0140-6736(78)90073-9)
42. Wolfe GI, Kaminski HJ, Aban IB, Minisman G, Kuo HC, Marx A et al (2019) Long-term effect of thymectomy plus prednisone versus prednisone alone in patients with non-thymomatous myasthenia gravis: 2-year extension of the MGTX randomised trial. *Lancet Neurol*. [https://doi.org/10.1016/S1474-4422\(18\)30392-2](https://doi.org/10.1016/S1474-4422(18)30392-2)
43. Xing L, Dai Z, Jabbari A, Cerise JE, Higgins CA, Gong W et al (2014) Alopecia areata is driven by cytotoxic T lymphocytes and is reversed by JAK inhibition. *Nat Med*. <https://doi.org/10.1038/nm.3645>
44. Yamada Y, Yoshida S, Suzuki H, Tagawa T, Iwata T, Mizobuchi T et al (2013) Efficacy of perioperative high-dose prednisolone therapy during thymectomy in myasthenia gravis patients. *J Cardiothorac Surg*. <https://doi.org/10.1186/1749-8090-8-226>
45. Yang Q, Zhang M, Chen Q, Chen W, Wei C, Qiao K et al (2020) Cutting edge: characterization of human tissue-resident memory T cells at different infection sites in patients with tuberculosis. *J Immunol*. <https://doi.org/10.4049/jimmunol.1901326>
46. Zenewicz LA, Yancopoulos GD, Valenzuela DM, Murphy AJ, Karow M, Flavell RA (2007) Interleukin-22 but not interleukin-17 provides protection to hepatocytes during acute liver inflammation. *Immunity*. <https://doi.org/10.1016/j.immuni.2007.07.023>
47. Zhang C-J, Gong Y, Zhu W, Qi Y, Yang C-S, Fu Y et al (2016) Augmentation of circulating follicular helper T cells and their impact on autoreactive B cells in myasthenia gravis. *J Immunol*. <https://doi.org/10.4049/jimmunol.1500725>
48. Zundler S, Becker E, Spocinska M, Slawik M, Parga-Vidal L, Stark R et al (2019) Hobit- and Blimp-1-driven CD4⁺ tissue-resident memory T cells control chronic intestinal inflammation. *Nat Immunol*. <https://doi.org/10.1038/s41590-018-0298-5>

Publisher's Note Springer Nature remains neutral with regard to jurisdictional claims in published maps and institutional affiliations.